

# Electrochemiluminescent immunoassay enhancement driven by carbon nanotubes†

Sara Rebecani,<sup>id</sup><sup>a</sup> Cecilia Wetzl,<sup>id</sup><sup>b</sup> Valeria Anna Zamolo,<sup>c</sup>  
Alejandro Criado,<sup>id</sup><sup>\*bd</sup> Giovanni Valenti,<sup>id</sup><sup>\*a</sup> Francesco Paolucci<sup>a</sup> and  
Maurizio Prato<sup>id</sup><sup>bce</sup>

**Electrochemiluminescence (ECL) is a leading analytical technique for clinical monitoring and early disease diagnosis. Carbon nanotubes are used as efficient nanomaterials for ECL signal enhancement providing new insights into the mechanism for the ECL generation but also affording application in bead-based immunoassay and ECL microscopy-based bioimaging.**

Biomarkers are biological indicators with a key role in identifying human body function changes. Recently, the quantitative detection of biomarkers has become even more important in clinical monitoring implementation and early screening of cancer and other diseases. More sensitive and specific sensors are developed for the detection of low concentrations of biomarkers in complex matrices like blood and other biofluids.<sup>1,2</sup> The quantification of biomarkers is essential in the management of the actual pandemic scenario and the prevention of future epidemics.<sup>3</sup>

In this context, electrochemiluminescence (ECL) is a leading technique in the field of immunoassay-based biomarker detection and biosensor fabrication.<sup>4-8</sup> The widespread use and growth of ECL are due to its advantageous features, such as satisfactory signal-to-noise ratio,<sup>9,10</sup> good spatial and temporal control and signal generation in an aqueous environment that allows analysis in real and complex matrices.<sup>11</sup> In commercial ECL-based immunoassays, such as Elecsys<sup>®</sup> immunoassays,<sup>12</sup>

the biomarkers are detected after their immobilization on the working electrode through magnetic beads, attracted to the electrode surface using a magnet.<sup>13</sup>

In this study, the ECL bead-based assay is combined with carbon nanotubes to optimize the ECL active layer and activate a more efficient ECL mechanism. Carbon nanotubes are unique nanomaterials largely used in ECL, especially for biosensors based on  $[\text{Ru}(\text{bpy})_3]^{2+}/\text{TPrA}$ .<sup>14-17</sup> However, the mechanism of ECL enhancement in bead-based assays remains underexplored. Here we exploit an ECL mechanism, activated by the presence of functionalized carbon nanotubes (f-CNT), to enhance the ECL signal.

ECL has been used, in combination with microscopy, as a surface confined technique for the visualization of objects<sup>18-23</sup> and for mapping and quantifying analytes at an electrode surface.<sup>24,25</sup> Although this technique shows great spatial resolution, it has to be optimized to further extend and control the thin layer from the electrode, in which the objects can be visualized, which is limited by the short lifetime of the electrogenerated coreactant radicals.<sup>26-28</sup> Therefore, different approaches have been applied for controlling the ECL active layer, underlining how promising the technique is for sensor applications.<sup>5,13,29-35</sup> For example, the application of the so-called Faraday cage for extending the ECL emission layer, in which luminophores become a part of the electrode, is an innovative and efficient approach for the improvement of the technique.<sup>36</sup> In this context, nanotechnologies have a pivotal role in the implementation of the ECL signal.<sup>37</sup> The successful and promising combination between carbon-based nanomaterials and ECL was deeply studied, owing to the unique and advantageous features, such as the fast kinetics for amine oxidation.<sup>30,38-42</sup>

Herein, functionalized carbon nanotubes were applied for optimizing the distribution of the ECL-emitting layer (see Fig. 1). This approach allows the increase of the ECL active layer and enhancement of the signal through a combination of two different ECL generation mechanisms. To mimic the real bead-based commercial immunoassays, the effect of f-CNT on micron-sized magnetic beads functionalized with a biotinylated

<sup>a</sup> Department of Chemistry Giacomo Ciamician, University of Bologna, via Selmi 2, Bologna 40126, Italy. E-mail: g.valenti@unibo.it

<sup>b</sup> Center for Cooperative Research in Biomaterials (CIC biomaGUNE), Basque Research and Technology Alliance (BRTA), Donostia-San Sebastián 20014, Spain

<sup>c</sup> Department of Chemical and Pharmaceutical Sciences, University of Trieste, Piazzale Europa, 1, Trieste 34127, Italy

<sup>d</sup> Universidade da Coruña, Centro de Investigacións Científicas Avanzadas (CICA), Rúa As Carballeiras, A Coruña, 15071, Spain. E-mail: a.criado@udc.es

<sup>e</sup> Ikerbasque, Basque Foundation for Science, Bilbao 48013, Spain

† Electronic supplementary information (ESI) available: Synthetic procedure of CNT-Ru, characterization analysis, ECL emission on beads with 4 μm diameter and with DBAE as coreactant, ECL from 2.8 μm beads with not-functionalized CNT, deconvolution, and movie of CV-ECL peaks. See DOI: 10.1039/d1cc03457j

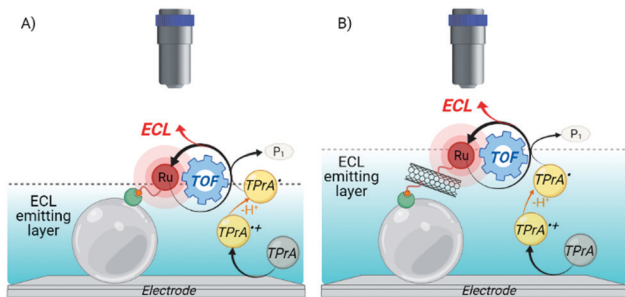
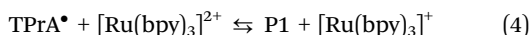
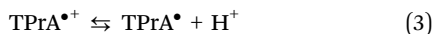
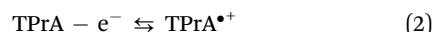
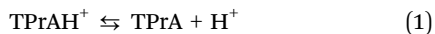


**Fig. 1** “Oxidative-reduction” coreactant mechanisms for the electrochemiluminescence emission of micromagnetic bead (light grey sphere) systems (biotin, red circle, and streptavidin, green shape), involving TPrA as coreactant and  $[\text{Ru}(\text{bpy})_3]^{2+}$  as luminophore. (A) Only TPrA is oxidized on the electrode. (B)  $[\text{Ru}(\text{bpy})_3]^{2+}$  is also oxidized on the double-walled carbon nanotubes (f-CNTs). Created with BioRender.com.

carbon nanotube labeled with a  $[\text{Ru}(\text{bpy})_3]^{2+}$  complex was investigated. Carbon nanotubes can create a conductive layer around the beads, extending the ECL active layer and enhancing the ECL signal through the direct oxidation of the luminophore on this new conductive layer. This latter mechanism is not active in a conventional bead system, in which the direct oxidation of the luminophores is neglected.<sup>13,43,44</sup>

The most important ECL application is based on the so-called “oxidative reduction” coreactant mechanism for ECL generation, in which TPrA is used as the sacrificial coreactant and tris(2, 2'-bipyridyl) ruthenium(II),  $[\text{Ru}(\text{bpy})_3]^{2+}$ , as the luminophore.<sup>43,45–47</sup> This mechanism was largely investigated and the species involved are the protagonists in the field of ECL biosensors and imaging for emission detection of objects close to the electrode surface (within 3  $\mu\text{m}$  from the electrode surface). The commercialized immunosystem involved micromagnetic beads functionalized with biotinylated antibodies labeled with  $[\text{Ru}(\text{bpy})_3]^{2+}$  and TPrA as coreactant.<sup>12,13</sup> In this mechanism, also called remote ECL, TPrA is oxidized (Fig. 1A) at the electrode to the corresponding radical cation  $\text{TPrA}^{\bullet+}$ , and  $\text{TPrA}^{\bullet+}$  radicals are produced after a deprotonation step (1–3).  $\text{TPrA}^{\bullet+}$  reduces the luminophore (4) that is subsequently oxidized to the excited state by  $\text{TPrA}^{\bullet+}$  (5)<sup>13,43</sup>



where P1 is the product of the homogeneous  $\text{TPrA}^{\bullet}$  oxidation.

According to the mechanism outlined above, because of the limited  $\text{TPrA}^{\bullet+}$  lifetime,<sup>13,43</sup> emission may only occur from luminophores located within a few micrometers ( $\sim 3 \mu\text{m}$ ) from the electrode surface; this is among the major intrinsic limiting factors for the signal intensity.<sup>48</sup> Additionally, the ECL distribution around the beads is not homogeneous, depending on the decaying radical distribution.<sup>13</sup> High intensity can, in principle,

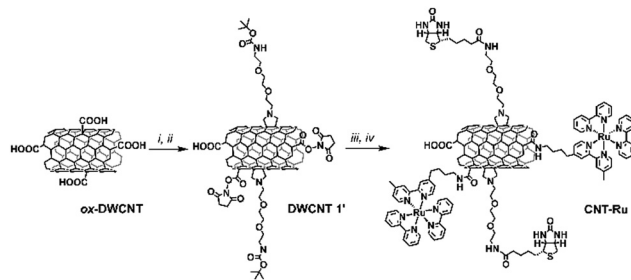


**Fig. 2** Schematic representation for the synthesis of f-CNTs labeled with  $[\text{Ru}(\text{bpy})_3]^{2+}$  and biotin (named CNT-Ru): (i): paraformaldehyde, BocNH-PEG2-NHCH<sub>2</sub>CO<sub>2</sub>H, DMF, 115 °C, r.t.; (ii): DIEA, EDC, DMF, r.t., 1 h; (iii): NHS, DMF, r.t., 15 h; (iv):  $[\text{Ru}(\text{bpy})_3]^{2+}$  amine derivative, 45 °C, 24 h; (v): HCl:1,4-dioxane (1/2), r.t.; 15 h; (vi): EDC, NHS, biotin, MES, r.t., 72 h.

be obtained by increasing the distance from the electrode surface, in which both radicals are present in sizeable amounts, and also to involve an increased fraction of fluorophores in the ECL-generating process.

In this context, functionalized carbon nanotubes (CNT-Ru) were prepared with a double functionalization of oxidized DWCNTs, by combining 1,3 dipolar cycloaddition reaction and amidation of carboxylic groups to sequentially introduce: (i) the  $[\text{Ru}(\text{bpy})_3]^{2+}$  complex as a luminophore, and (ii) an amine functional group to link biotin as a biorecognition element (Fig. 2 and Fig. S1, S2, ESI<sup>†</sup>). Thus, the biotin moiety is used for the attachment of this material onto micromagnetic beads. The above approach provided tubes with a controllable labeling capability and high surface area, and whose electronic properties were still highly preserved. As such, they proved to promote the fast electrochemical oxidation of amines very efficiently, once deposited onto the electrode surface. Fluorescence spectra and mass analysis confirmed the functionalization of CNTs (Fig. S3 and Table S1, ESI<sup>†</sup>), whose structure was analyzed by TEM imaging, TGA, and Raman spectroscopy (Fig. S4–S6, ESI<sup>†</sup>).

CNT-Ru was used for micromagnetic beads functionalization through biotin-streptavidin strong bonding (beads@CNT-Ru Fig. S5–S7, ESI<sup>†</sup>). The functionalized beads were then immobilized by a magnet onto a platinum electrode and their ECL emission was integrated using an ECL-microscope in the presence of 180 mM of TPrA. The ECL emission from beads@CNT-Ru was then compared with that measured on standard 2.8  $\mu\text{m}$  microbeads functionalized with a biotinylated antibody labeled with  $[\text{Ru}(\text{bpy})_3]^{2+}$  complex (beads@Ru).

An increase of  $\sim 4$  times in the ECL intensity integrated over single beads@CNT-Ru (Fig. 3A and Fig. S8, ESI<sup>†</sup>) was obtained compared with beads@Ru (Fig. 3B), suggesting that CNTs played a relevant role in the ECL signal enhancement. The increased intensity is demonstrated by comparing the profiles in Fig. 3C, in which the turnover frequencies (TOF), *i.e.*, the normalized signals considering the different luminophore loadings between the two types of beads are also reported. TOF is the number of photons emitted in 1 s by a single luminophore, which is obtained by dividing the integrated ECL emission from the single bead by the number of luminophores present on the bead surface and by the integration time (see also ESI<sup>†</sup> and Fig. S9). TOF for

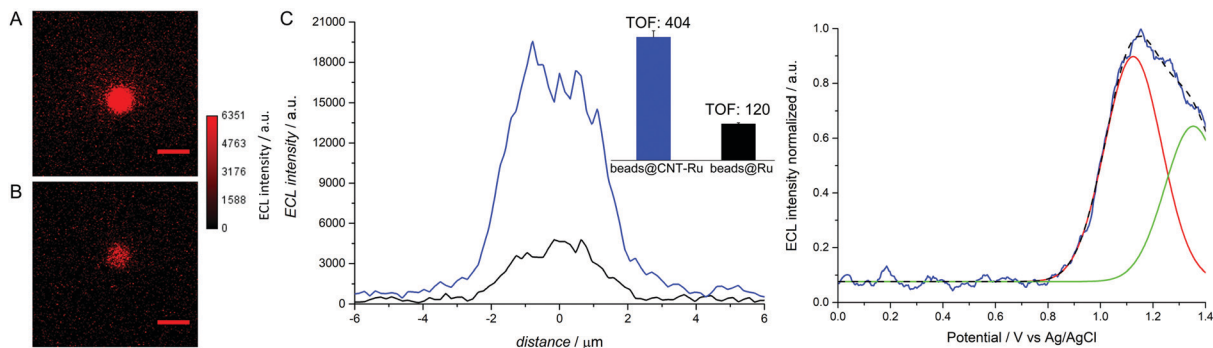


**Fig. 3** (A) ECL imaging of 2.8  $\mu\text{m}$  single-beads labeled with CNTs labeled with  $[\text{Ru}(\text{bpy})_3]^{2+}$  (beads@CNT-Ru) and (B) with biotinylated antibody functionalized with  $[\text{Ru}(\text{bpy})_3]^{2+}$  (beads@Ru). The images were obtained by applying a constant potential of 1.4 V (vs. Ag/AgCl) for 4 s in 180 mM TPrA and 0.2 M phosphate buffer (PB). Pt wire was used as a counter electrode. The EMCCD camera was coupled with a potentiostat. Integration time, 8 s; magnification, X100; scale bar, 5  $\mu\text{m}$ . (C) Comparison of the bead profile lines (black line, beads@Ru; blue line, beads@CNT-Ru). Inset of the comparison between TOF values calculated for beads@Ru (black) and beads@CNT-Ru (blue). Error bars show the standard error ( $n \geq 10$ ). (D) Cyclic voltammetry performed on beads@CNT-Ru (blue), scanning the potential between 0 V and 1.4 V and the ECL emission signal acquired each 200 ms. Deconvolution of the cyclic voltammetry peak at 1 V (red line) and 1.2 V (green line), in which the TPrA and  $[\text{Ru}(\text{bpy})_3]^{2+}$  were oxidized, respectively. The sum of these two peak deconvolutions was represented by the dotted black line. The EMCCD camera was coupled with a potentiostat. Integration time, 200 ms.

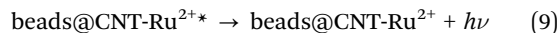
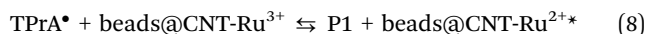
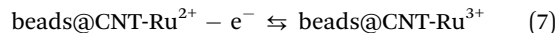
beads@CNT-Ru increased by 70% compared to that of beads@Ru, thus confirming the strategic role played by CNTs in promoting enhanced ECL signals.

Notice that TOF is normalized for the quantity of luminophore as it is described in detail in the ESI†. A possible explanation for the observed effect is associated with the previously observed ability of CNTs to promote the efficient anodic oxidation of amines and other substrates.<sup>37,49–53</sup> As shown in Fig. 1A and according to the mechanism outlined above (remote ECL, eqn (1)–(6)), the ECL signal depends entirely on the direct oxidation of TPrA. The CNT-Ru moieties, which are randomly distributed onto the bead surface, are likely to form a conductive electrocatalytic network, in turn electronically wired to the electrode surface, onto which TPrA oxidation may occur. This leads to an effective increase of the TPrA radicals' concentration over the whole bead surface compared with beads@Ru, in which oxidation only occurs at the electrode surface.

To confirm the above hypothesis, ECL analysis at a single-bead level was investigated substituting TPrA with dibutylaminoethanol (DBAE) as the coreactant (Fig. S10, ESI†). In the ECL generation mechanism, DBAE exhibited an analogous mechanism as depicted by eqn (1)–(6). However, due to the very short lifetime of the DBAE radical cation,<sup>48</sup> emission from beads@Ru was not observed. In contrast, in the case of beads@CNT-Ru, the presence of the CNT electrocatalytic network, at a very short distance from the luminophore, allows the sequence of processes in eqn (1)–(6) along with the observation of a strong signal (Fig. S10, ESI†).

Quite unexpectedly, the analysis of the ECL signal distribution with the applied potential, as measured by acquiring the ECL signal from the individual beads (either beads@Ru or beads@CNT-Ru) during a cyclic potential scan from 0 to 1.4 V (acquisition time 200 ms), also highlighted an additional ECL generation mechanism (see the ESI†, Movie). Fig. 3D illustrates the analysis of the case in which beads@CNT-Ru is leading an

additional contribution at  $\sim 1.2\text{--}1.4$  V compared with the curves related to beads@Ru (Fig. S11, ESI†). It may be associated with the anodic oxidation of the  $[\text{Ru}(\text{bpy})_3]^{2+}$  moieties also supported by the comparison between the electrochemical behaviour of beads@CNT-Ru and beads@Ru in the absence of coreactant (see Fig. S12, ESI†). Such an oxidation process would occur onto the CNT surface because of the flexibility of the linker connecting the luminophore to the CNT moiety, allowing an alternative mechanism for ECL generation which is not viable with beads@Ru. Such a mechanism involves both TPrA (eqn (1)–(3)) and  $[\text{Ru}(\text{bpy})_3]^{2+}$  (eqn (7)–(9)), whose parallel oxidation leads to ECL, according to the following mechanism where the homogeneous reactions eqn (4) and (5) are replaced by eqn (7) and (8).



This mechanism is usually observed in the homogeneous case, in which both luminophore and coreactant are free to diffuse to the electrode surface. However, this is not possible for the heterogeneous ECL, in which remote ECL is usually the only mechanism observed.<sup>43</sup> Fundamental characters in the ECL generation remain the presence of the luminophore onto the beads (Fig. S13, ESI†) and the application of a sufficiently high oxidation potential for overcoming the ohmic drop due to the high concentration of coreactant.<sup>13</sup>

Finally, the effective role played by the conductive network of CNTs in promoting enhanced ECL around the beads was further confirmed by inspecting the emission of the 4  $\mu\text{m}$  diameter beads, similarly functionalized with either CNT-Ru or Ru labels (Fig. S14A and B, ESI†). The former displays a more homogeneous emission over the entire bead and larger ECL intensity compared with the latter (Fig. S14C, ESI†).

In conclusion, the insertion of CNTs (DWCNTs) as an interlayer between the luminophores and the magnetic microbead brings a significant enhancement of the ECL signal, which is a combined effect of the increased efficiency of the remote ECL mechanism, usually involved in such systems, and the concurrence of an additional ECL-generating mechanism, generally limited to homogeneous systems. A new and very promising route is opened for increasing the sensitivity of ECL immunoassays based on the ECL imaging technique.

This work was supported by MIUR, grant number 2017 PBXPN4. M. P., as the recipient of the AXA Bionanotechnology Chair, is grateful to the AXA Research Fund for financial support. This work was performed under the Maria de Maeztu Units of Excellence Program from the Spanish State Research Agency – Grant No. MDM-2017-0720. A. C. thanks Xunta de Galicia for his research grant Atracción de Talento (no. ED431H 2020/17).

## Conflicts of interest

The authors declare no competing financial interest.

## References

- 1 Y. Bai, T. Shu, L. Su and X. Zhang, *Anal. Bioanal. Chem.*, 2020, **412**, 6655–6665.
- 2 M. Sharifi, M. R. Avadi, F. Attar, F. Dashtestani, H. Ghorchian, S. M. Rezayat, A. A. Saboury and M. Falahati, *Biosens. Bioelectron.*, 2019, **126**, 773–784.
- 3 L. Xu, D. Li, S. Ramadan, Y. Li and N. Klein, *Biosens. Bioelectron.*, 2020, **170**, 112673.
- 4 H. Qi and C. Zhang, *Anal. Chem.*, 2020, **92**, 524–534.
- 5 C. Ma, Y. Cao, X. Gou and J.-J. Zhu, *Anal. Chem.*, 2020, **92**, 431–454.
- 6 A. Juzgado, A. Soldà, A. Ostric, A. Criado, G. Valenti, S. Rapino, G. Conti, G. Fracasso, F. Paolucci and M. Prato, *J. Mater. Chem. B*, 2017, **5**, 6681–6687.
- 7 B. Babamiri, D. Bahari and A. Salimi, *Biosens. Bioelectron.*, 2019, **142**, 111530.
- 8 H. Li, L. Bouffier, S. Arbault, A. Kuhn, C. F. Hogan and N. Sojic, *Electrochem. Commun.*, 2017, **77**, 10–13.
- 9 M. Hesari and Z. Ding, *J. Electrochem. Soc.*, 2016, **163**, H3116–H3131.
- 10 M. M. Richter, *Chem. Rev.*, 2004, **104**, 3003–3036.
- 11 W. Miao, *Chem. Rev.*, 2008, **108**, 2506–2553.
- 12 Roche Diagnostic corporation.
- 13 A. Zanut, A. Fiorani, S. Canola, T. Saito, N. Ziebart, S. Rapino, S. Rebecani, A. Barbon, T. Irie, H.-P. Josel, F. Negri, M. Marcaccio, M. Windfuhr, K. Imai, G. Valenti and F. Paolucci, *Nat. Commun.*, 2020, **11**, 2668.
- 14 H. Wang, L. Liao, Y. Chai and R. Yuan, *Biosens. Bioelectron.*, 2020, **150**, 111915.
- 15 Y. Liu, Y. Sun and M. Yang, *Anal. Methods*, 2021, **13**, 903–909.
- 16 X. Wang, L. Yu, Q. Kang, L. Chen, Y. Jin, G. Zou and D. Shen, *Electrochim. Acta*, 2020, **360**, 136992.
- 17 C. Song, X. Li, L. Hu, T. Shi, D. Wu, H. Ma, Y. Zhang, D. Fan, Q. Wei and H. Ju, *ACS Appl. Mater. Interfaces*, 2020, **12**, 8006–8015.
- 18 H. Ding, W. Guo and B. Su, *Angew. Chem.*, 2020, **132**, 457–464.
- 19 G. Valenti, S. Scarabino, B. Goudeau, A. Lesch, M. Jović, E. Villani, M. Sentic, S. Rapino, S. Arbault, F. Paolucci and N. Sojic, *J. Am. Chem. Soc.*, 2017, **139**, 16830–16837.
- 20 L. C. Soulsby, D. J. Hayne, E. H. Doeven, L. Chen, C. F. Hogan, E. Kerr, J. L. Adcock and P. S. Francis, *ChemElectroChem*, 2018, **5**, 1543–1547.
- 21 H. Ding, W. Guo and B. Su, *Angew. Chem., Int. Ed.*, 2020, **59**, 449–456.
- 22 W. Zhao, H.-Y. Chen and J.-J. Xu, *Chem. Sci.*, 2021, **12**, 5720–5736.
- 23 H. Ding, P. Zhou, W. Fu, L. Ding, W. Guo and B. Su, *Angew. Chem., Int. Ed.*, 2021, **60**, 11769–11773.
- 24 L. Xu, Y. Li, S. Wu, X. Liu and B. Su, *Angew. Chem., Int. Ed.*, 2012, **51**, 8068–8072.
- 25 K. Kadimisetty, I. M. Mosa, S. Malla, J. E. Satterwhite-Warden, T. M. Kuhns, R. C. Faria, N. H. Lee and J. F. Rusling, *Biosens. Bioelectron.*, 2016, **77**, 188–193.
- 26 S. Voci, B. Goudeau, G. Valenti, A. Lesch, M. Jović, S. Rapino, F. Paolucci, S. Arbault and N. Sojic, *J. Am. Chem. Soc.*, 2018, **140**, 14753–14760.
- 27 F.-R. F. Fan and A. J. Bard, *Nano Lett.*, 2008, **8**, 1746–1749.
- 28 Z. Chen and Y. Zu, *J. Phys. Chem. C*, 2008, **112**, 16663–16667.
- 29 Z. Guo, Y. Sha, Y. Hu, Z. Yu, Y. Tao, Y. Wu, M. Zeng, S. Wang, X. Li, J. Zhou and X. Su, *Anal. Bioanal. Chem.*, 2016, **408**, 7203–7211.
- 30 J. Lu, L. Wu, Y. Hu, S. Wang and Z. Guo, *J. Electrochem. Soc.*, 2017, **164**, B421–B426.
- 31 C. Ma, M.-X. Wang, H.-F. Wei, S. Wu, J.-R. Zhang, J.-J. Zhu and Z. Chen, *Chem. Commun.*, 2021, **57**, 2168–2171.
- 32 A. Zanut, A. Fiorani, S. Rebecani, S. Kesarkar and G. Valenti, *Anal. Bioanal. Chem.*, 2019, **411**, 4375–4382.
- 33 A. Fiorani, D. Han, D. Jiang, D. Fang, F. Paolucci, N. Sojic and G. Valenti, *Chem. Sci.*, 2020, **11**, 10496–10500.
- 34 W. Guo, P. Zhou, L. Sun, H. Ding and B. Su, *Angew. Chem., Int. Ed.*, 2021, **60**, 2089–2093.
- 35 H. Ju, N. Wang, H. Gao, Y. Li, G. Li, W. Chen, Z. Jin, J. Lei and Q. Wei, *Angew. Chem., Int. Ed.*, 2021, **60**, 197–201.
- 36 Z. Guo, Y. Sha, Y. Hu and S. Wang, *Chem. Commun.*, 2016, **52**, 4621–4624.
- 37 A. Fiorani, J. P. Merino, A. Zanut, A. Criado, G. Valenti, M. Prato and F. Paolucci, *Curr. Opin. Electrochem.*, 2019, **16**, 66–74.
- 38 A. Zanut, F. Palomba, M. Rossi Scota, S. Rebecani, M. Marcaccio, D. Genovese, E. Rampazzo, G. Valenti, F. Paolucci and L. Prodi, *Angew. Chem., Int. Ed.*, 2020, **59**, 21858–21863.
- 39 G. Valenti, A. Fiorani, H. Li, N. Sojic and F. Paolucci, *ChemElectroChem*, 2016, **3**, 1990–1997.
- 40 G. Valenti, E. Rampazzo, S. Kesarkar, D. Genovese, A. Fiorani, A. Zanut, F. Palomba, M. Marcaccio, F. Paolucci and L. Prodi, *Coord. Chem. Rev.*, 2018, **367**, 65–81.
- 41 S. Voci, H. Al-Kutubi, L. Rassaei, K. Mathwig and N. Sojic, *Anal. Bioanal. Chem.*, 2020, **412**, 4067–4075.
- 42 S. Zhang, R. Geryak, J. Geldmeier, S. Kim and V. V. Tsukruk, *Chem. Rev.*, 2017, **117**, 12942–13038.
- 43 W. Miao, J.-P. Choi and A. J. Bard, *J. Am. Chem. Soc.*, 2002, **124**, 14478–14485.
- 44 P. Dutta, D. Han, B. Goudeau, D. Jiang, D. Fang and N. Sojic, *Biosens. Bioelectron.*, 2020, **165**, 112372.
- 45 J. K. Leland and M. J. Powell, *J. Electrochem. Soc.*, 1990, **137**, 3127–3131.
- 46 Y. Zu and A. J. Bard, *Anal. Chem.*, 2000, **72**, 3223–3232.
- 47 L. S. Dolci, S. Zanarini, L. Della Ciana, F. Paolucci and A. Roda, *Anal. Chem.*, 2009, **81**, 6234–6241.
- 48 M. Sentic, M. Milutinovic, F. Kanoufi, D. Manojlovic, S. Arbault and N. Sojic, *Chem. Sci.*, 2014, **5**, 2568–2572.
- 49 G. Valenti, M. Zangheri, S. E. Sansaloni, M. Mirasoli, A. Penicaud, A. Roda and F. Paolucci, *Chem. – Eur. J.*, 2015, **21**, 12640–12645.
- 50 V. A. Zamolo, G. Valenti, E. Venturelli, O. Chaloin, M. Marcaccio, S. Boscolo, V. Castagnola, S. Sosa, F. Berti, G. Fontanive, M. Poli, A. Tubaro, A. Bianco, F. Paolucci and M. Prato, *ACS Nano*, 2012, **6**, 7989–7997.
- 51 R. Wang, H. Wu, R. Chen and Y. Chi, *Small*, 2019, **15**, 1901550.
- 52 L. Yang, A. D. Hendsbee, Q. Xue, S. He, C. R. De-Jager, G. Xie, G. C. Welch and Z. Ding, *ACS Appl. Mater. Interfaces*, 2020, **12**, 51736–51743.
- 53 K. Kadimisetty, S. Malla, K. S. Bhalerao, I. M. Mosa, S. Bhakta, N. H. Lee and J. F. Rusling, *Anal. Chem.*, 2018, **90**, 7569–7577.